Supplementary material

Well-defined Fe-Cu diatomic sites for efficient catalysis of CO_2 electroreduction

Manman Feng [a], Xuemei Wu [a]*, Huiyuan Cheng [a], Zihao Fan [a], Xiangcun Li [a], Fujun Cui [b], Shuai Fan [a], Yan Dai [b], Guangping Lei [c], Gaohong He [a,b]*

[a] State Key Laboratory of Fine Chemicals, Research and Development Center of Membrane Science and Technology, School of Chemical Engineering, Dalian University of Technology, Linggong Road, Dalian 116024, China

[b] Panjin Institute of Industrial Technology, Dalian University of Technology, Panjin 124221, Liaoning, China

[c] Research Center of Shanxi Province for Solar Energy Engineering and Technology, School of Energy and power Engineering, North University of China, Taiyuan 030051, China

*Corresponding author: xuemeiw@dlut.edu.cn (X. Wu), hgaohong@dlut.edu.cn (G. He)

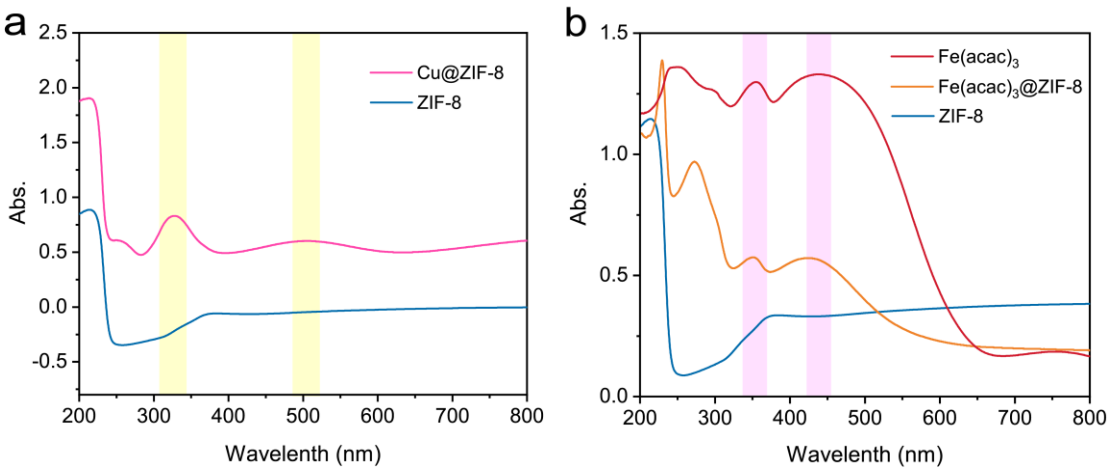

Fig. S1. Diffuse reflectance ultraviolet-visible absorption spectra of Cu@ZIF-8, $Fe(acac)_3$@ZIF-8, $Fe(acac)_3$ powder and ZIF-8.

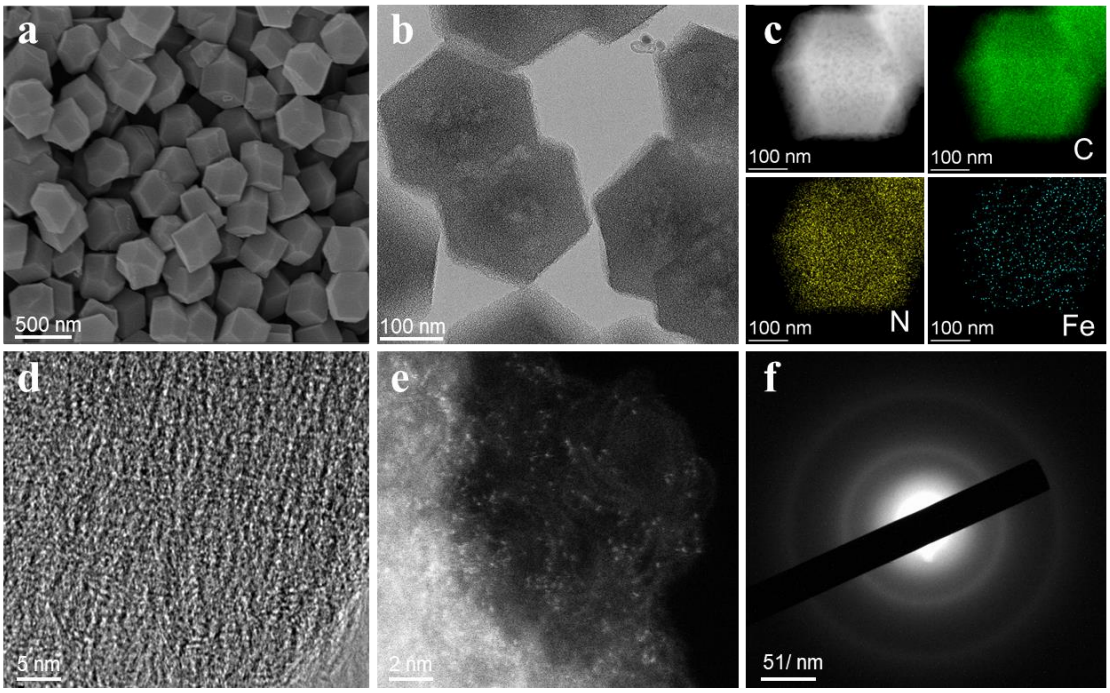

Fig. S2. (a) SEM image, (b) TEM image, (c) EDS mapping, (d) HRTEM image, (e) HAADF-STEM image, and (f) SAED pattern of Fe-N-C.

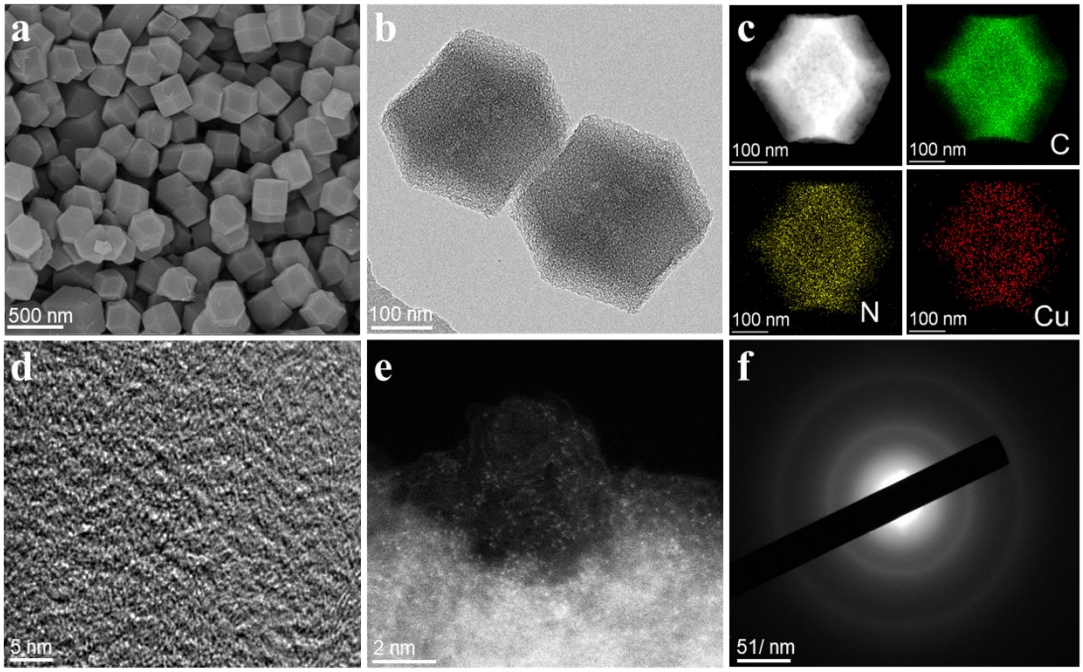

Fig. S3. (a) SEM, image (b) TEM image, (c) EDS mapping, (d) HRTEM image, (e) HAADF-STEM image, and (f) SAED pattern of Cu-N-C.

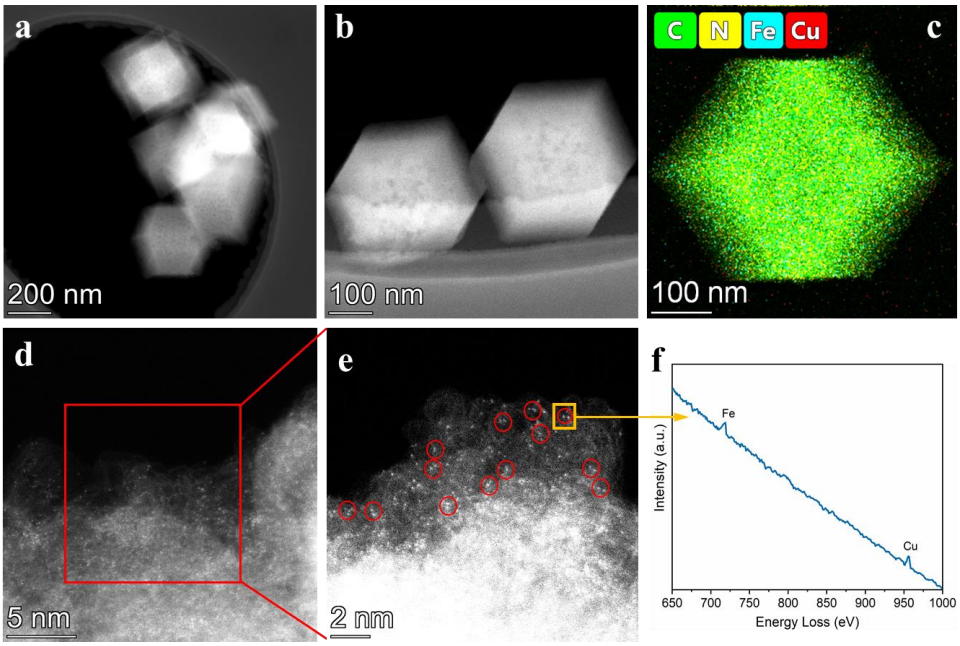

Fig. S4. (a), (b), (d) and (e) HAADF-STEM images of Fe/Cu-N-C and (c) corresponding EDS mapping, (f) EELS spectrum.

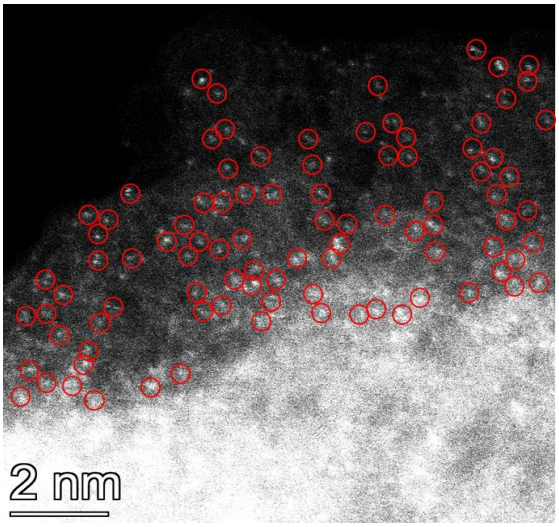

Fig. S5. HAADF-STEM images of Fe/Cu-N-C.

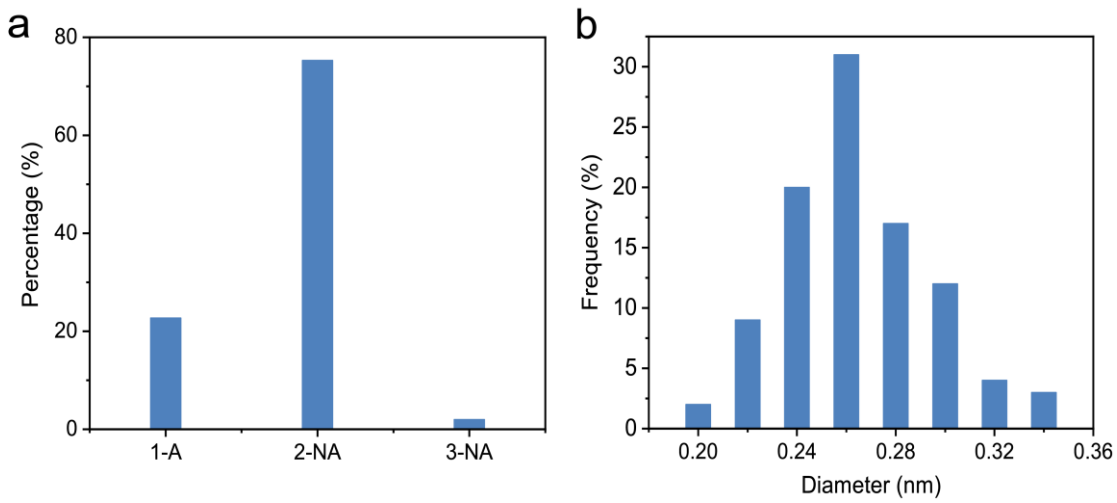

Fig. S6. (a) Percentage of isolated atoms, 2 neighboring atoms and 3 neighboring atoms in Fe/Cu-N-C.

(b) Statistical distance between 2 neighboring monomers.

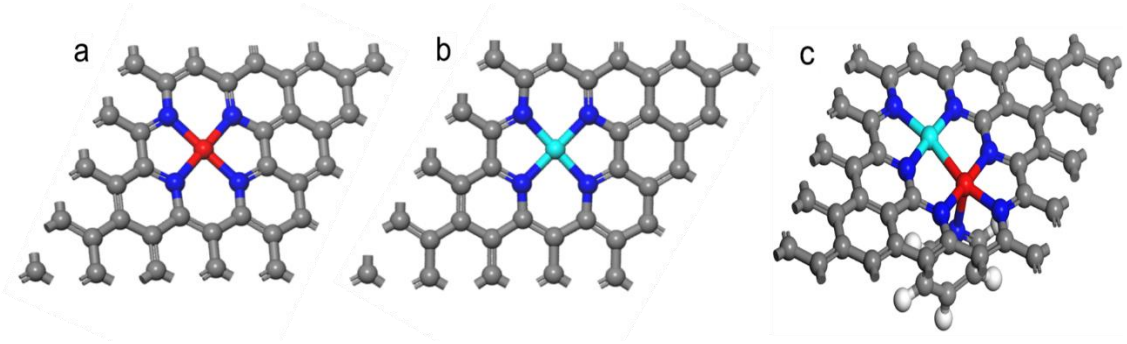

Fig. S7. Scheme of (a) Fe-N-C, (b) Cu-N-C and (c) Fe/Cu-N-C in DFT calculations.

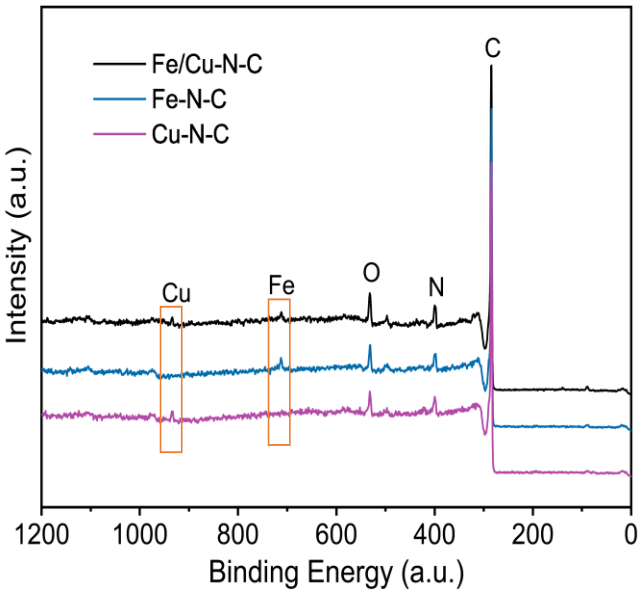

Fig. S8. XPS survey spectra of Fe/Cu-N-C, Fe-N-C, and Cu-N-C.

Table S1. Elemental compositions of various catalyst samples, as measured using XPS.

Sample	C (at%)	N (at%)	O (at%)	Cu (at%)	Fe (at%)
N-C	90.92	5.64	3.44	0	0
Cu-N-C	90.95	5.65	3.02	0.38	0
Fe-N-C	89.21	6.02	4.34	0	0.43
Fe/Cu-N-C	89.14	5.70	4.69	0.18	0.29

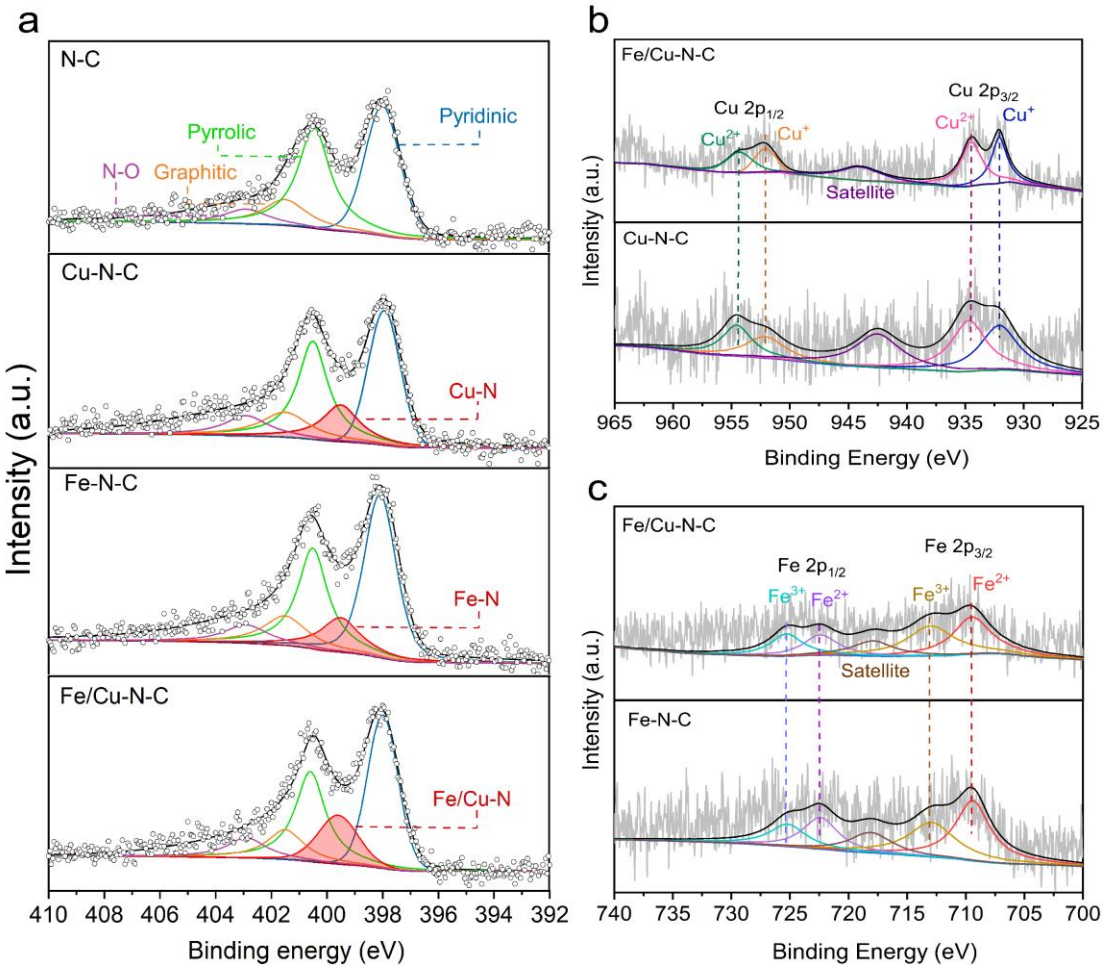

Fig. S9. High-resolution XPS spectra of various catalyst samples: (a) N 1s, (b) Cu 2p, and (c) Fe 2p.

Table S2. N 1s components in catalyst samples, as determined by fitting of the corresponding XPS data.

Sample	Pyridinic N (%)	M-N (%)	Pyrrolic N (%)	Graphitic N (%)	Oxide N (%)
N-C	39.34	0	39.13	13.72	7.81
Cu-N-C	31.71	14.56	31.22	13.02	9.49
Fe-N-C	36.32	15.36	28.45	12.18	7.69
Fe/Cu-N-C	34.31	19.31	26.01	11.81	8.56

Table S3. Fitting results for N 1s derived from corresponding XPS data.

Sample	Pyridinic N (%)	M-N (%)	Pyrrolic N (%)	Graphitic N (%)	Oxide N (%)
Fe/Cu-N-C 900℃	39.34	15.68	21.67	11.35	11.96
Fe/Cu-N-C 1000℃	34.31	19.31	26.01	11.81	8.56
Fe/Cu-N-C 1100℃	33.66	21.36	16.91	16.82	11.25
Fe/Cu-N-C 1200℃	32.47	22.31	26.01	18.06	11.35

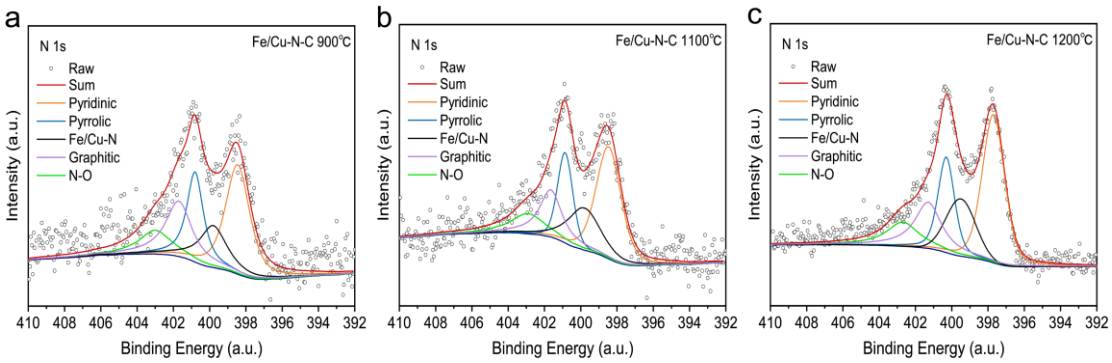

Fig. S10. (a), (b), (c) high resolution N 1 s XPS spectra of Fe/Cu-Nx-C (T).

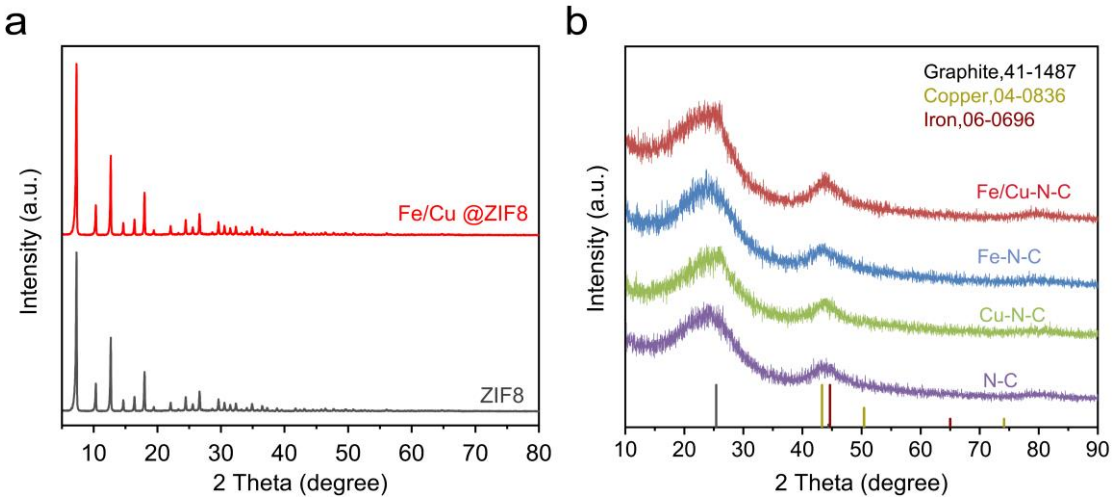

Fig. S11. XRD patterns of (a) Fe/Cu-codoped ZIF-8 and ZIF-8, and (b) Fe/Cu-N-C, Fe-N-C, Cu-N-C, and N-C catalysts.

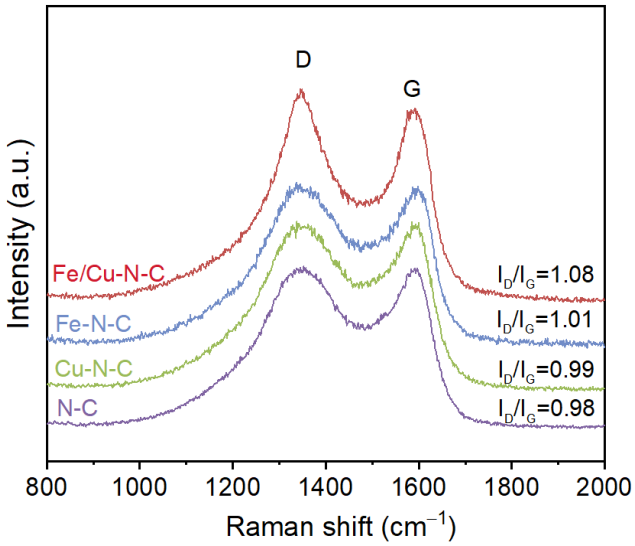

Fig. S12. Raman spectra of N-C, Cu-N-C, Fe-N-C, and Fe/Cu-N-C.

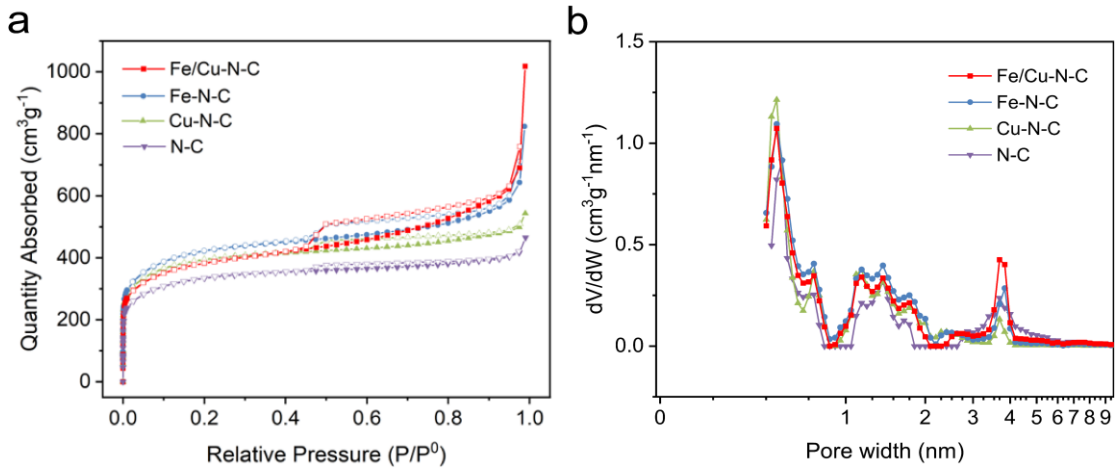

Fig. S13. (a) Nitrogen adsorption/desorption isotherms and (b) pore size distributions of Fe/Cu-N-C, Fe-N-C, Cu-N-C, and N-C.

Table S4. BET surface areas and pore volumes of catalyst samples.

Sample	BET surface area ($cm^2 g^{-1}$)	Micropore surface area ($cm^2 g^{-1}$)	External surface area ($cm^2 g^{-1}$)	V_{total} ($cm^3 g^{-1}$)	V_{μ} ($cm^3 g^{-1}$)
N-C	1216.2	1079.6	136.7	0.719	0.468
Cu-N-C	1392.5	1007.8	384.6	0.840	0.429
Fe-N-C	1521.2	1264.1	257.2	1.274	0.550
Fe/Cu-N-C	1541.9	1277.5	264.4	1.575	0.569

Table S5. Elemental compositions of catalysts, as determined by ICP-OES.

Sample	Fe (wt%)	Cu (wt%)
Cu-N-C	0	0.41
Fe-N-C	0.57	0
Fe/Cu-N-C	0.30	0.19

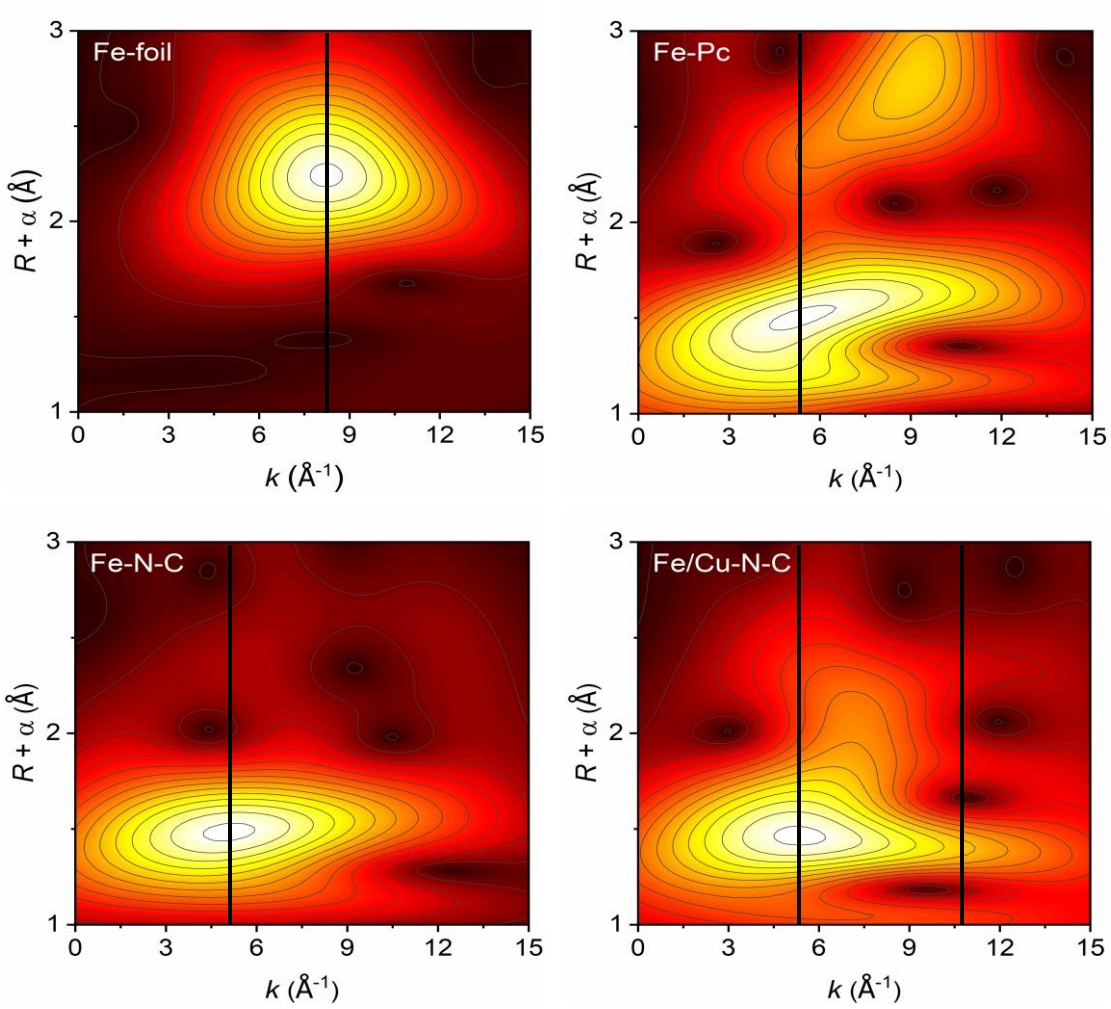

Fig. S14. WT plots of Fe/Cu-N-C, Fe-N-C, Fe Pc, and Fe foil.

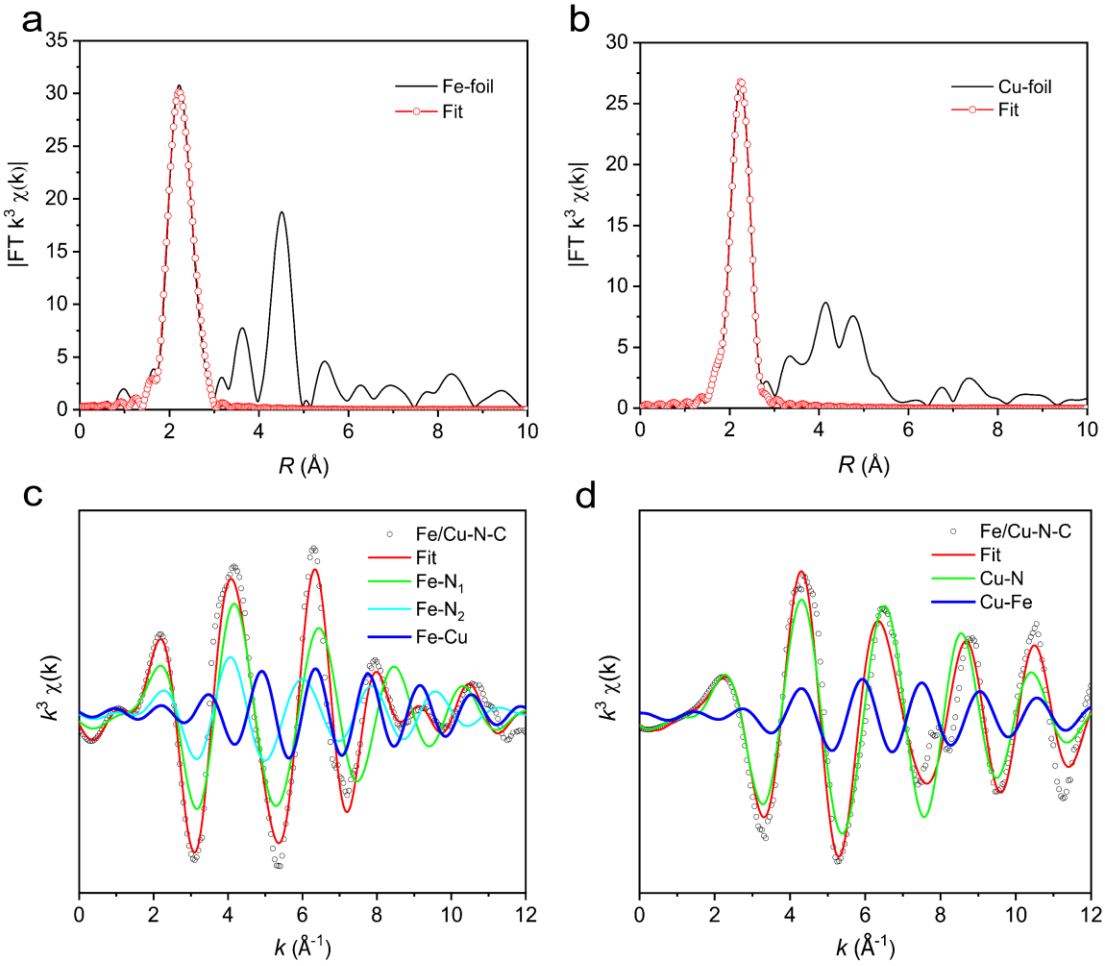

Fig. S15. K-edge EXAFS data and fitting for (a) Fe foil and (b) Cu foil; (c,d) EXAFS k-space fitting for Fe/Cu-N-C.

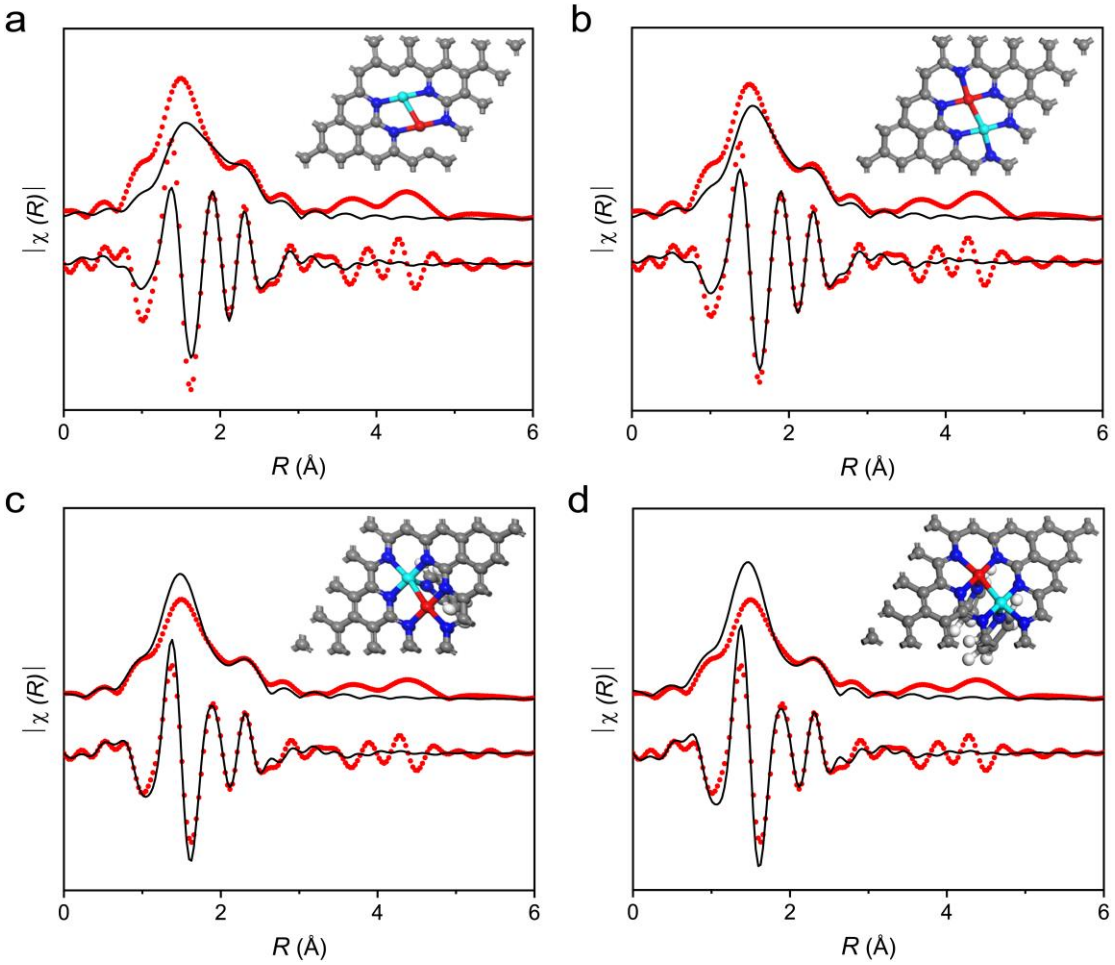

Fig. S16. Fitting of Fourier transformations of EXAFS spectra for Fe/Cu-N-C with different models:

(a) N_2Fe-CuN_3, (b) N_3Fe-CuN_3, (c) N_3Fe-CuN_4 and (d) N_4Fe-CuN_4.

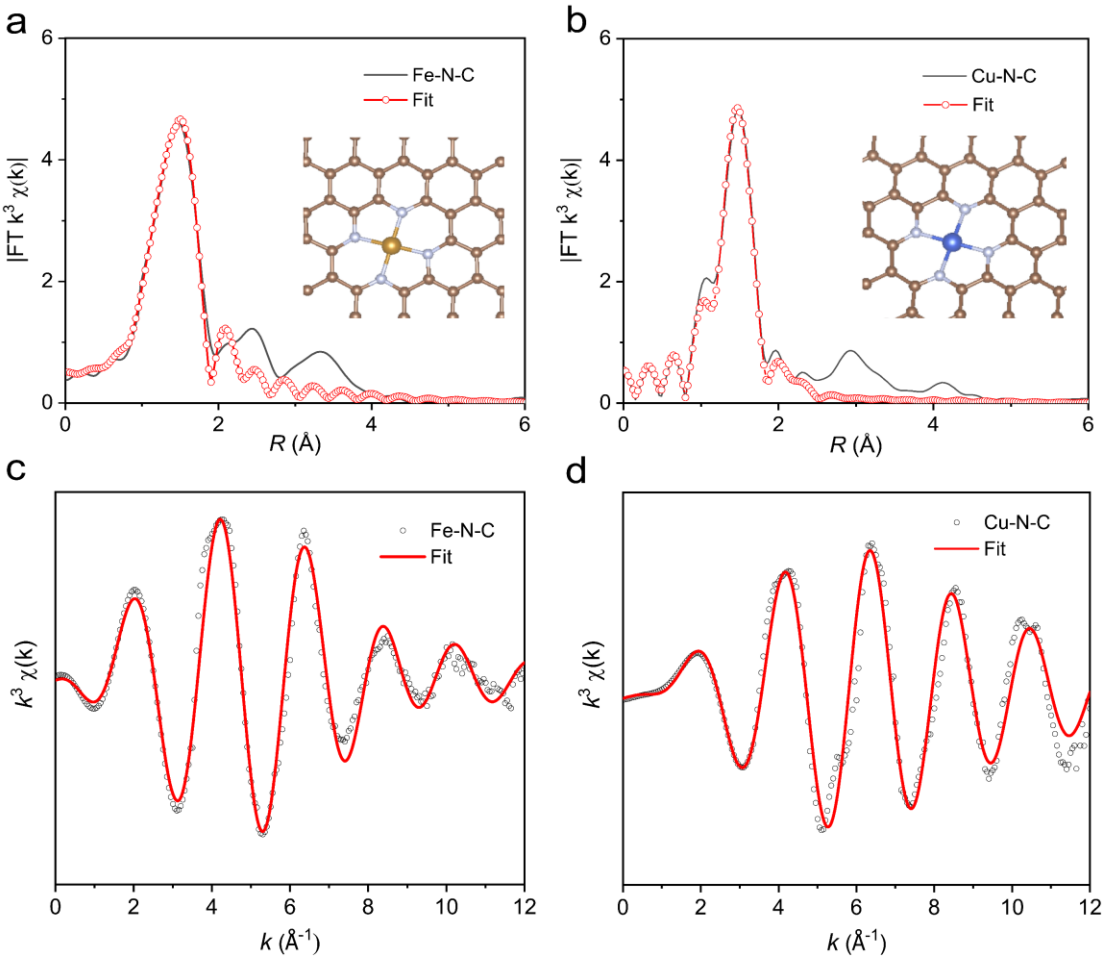

Fig. S17. EXAFS fitting for (a) Fe-N-C and (b) Cu-N-C in R space and corresponding EXAFS k-space fitting for (c) Fe-N-C and (d) Cu-N-C.

Table S6. Structural parameters for the catalyst samples obtained from the Cu K-edge EXAFS fitting ($S_0^2 = 0.83$).

Catalyst	Scattering pair	CN	*R* (Å)	σ^2 (10^{-3} Å^2)	Δ E_0 (eV)	R factor
Cu	Cu-Cu	12*	2.54 ± 0.01	8.6 ± 0.3	4.7 ± 0.5	0.0033
Cu-N-C	Cu-N	4.0 ± 0.1	1.95 ± 0.01	6.3 ± 0.5	−4.7 ± 0.3	0.002
Fe/Cu-N-C	Cu-N	3.0 ± 0.2	1.93 ± 0.01	6.6 ± 0.7	−4.9 ± 1.8	0.0015
	Cu-Fe	1.0 ± 0.3	2.59 ± 0.02	9.0 ± 2.6	1.3 ± 0.6	0.0015

CN: coordination number; *R*: bond distance; σ^2: Debye–Waller factor; ΔE_0: inner potential correction; R factor: goodness of fit. S_0^2 was set to 0.83 based on the experimental EXAFS fit for the Cu foil reference by fixing CN at the known crystallographic value.

Table S7. Structural parameters for the catalyst samples obtained from the Fe K-edge EXAFS fitting ($S_0^2 = 0.77$).

Catalyst	Scattering pair	CN	*R* (Å)	σ^2 (10^{-3} Å^2)	Δ E_0 (eV)	R factor
Fe foil	Fe-Fe	8*	2.46 ± 0.01	4.5 ± 0.6	5.6 ± 1.1	0.0061
Fe-N-C	Fe-N	4.3 ± 0.1	1.99 ± 0.01	5.9 ± 1.6	−0.6 ± 1.5	0.015
Fe/Cu-N-C	Fe-N1	3.0 ± 0.2	1.97 ± 0.01	4.3 ± 0.9	−2.1 ± 0.9	0.015
	Fe-N2	1.1 ± 0.1	2.13 ± 0.01	1.8 ± 1.4	9.5 ± 1.4	0.015
	Fe-Cu	1.0 ± 0.2	2.58 ± 0.01	7.5 ± 1.6	8.1 ± 1.6	0.015

CN: coordination number; *R*: bond distance; σ^2: Debye–Waller factor; ΔE_0: inner potential correction; R factor: goodness of fit. S_0^2 was set to 0.77 based on the experimental EXAFS fit for the Fe foil reference by fixing CN at the known crystallographic value.

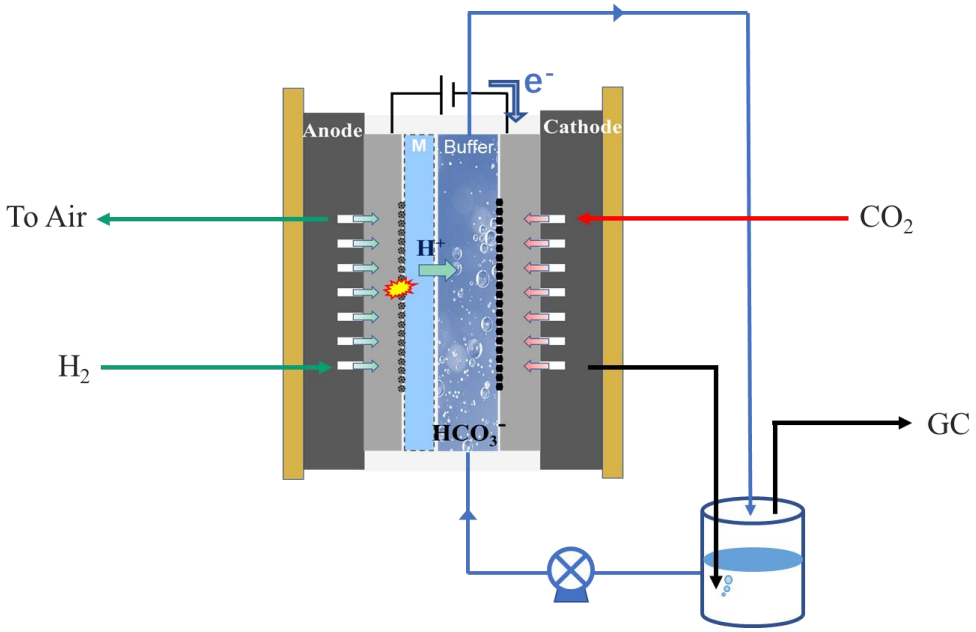

Fig. S18. Schematic diagram of electrochemical hydrogen pump device.

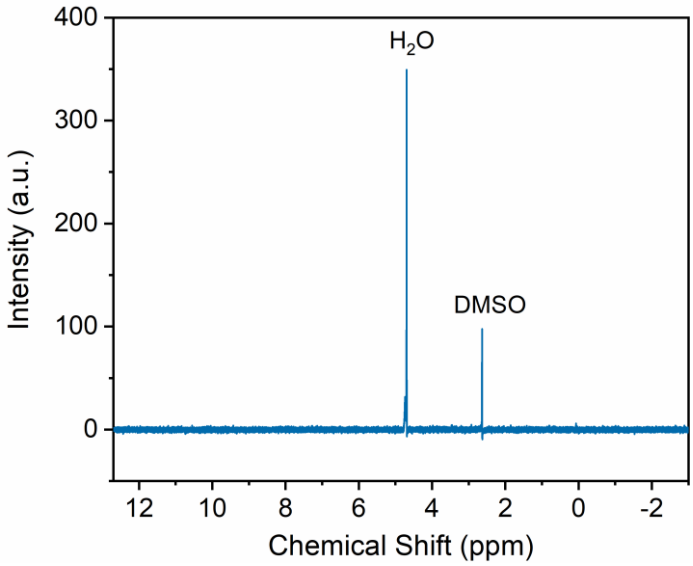

Fig. S19. ^{1}H NMR spectrum of the liquid product obtained over Fe/Cu-N-C after 1 h CO_2 reduction at −0.8 V.

Table S8. Elemental compositions of 0.5Fe-N-C catalyst, as determined by ICP-OES.

Sample	Fe (wt%)	Cu (wt%)
0.5Fe-N-C	0.32	0

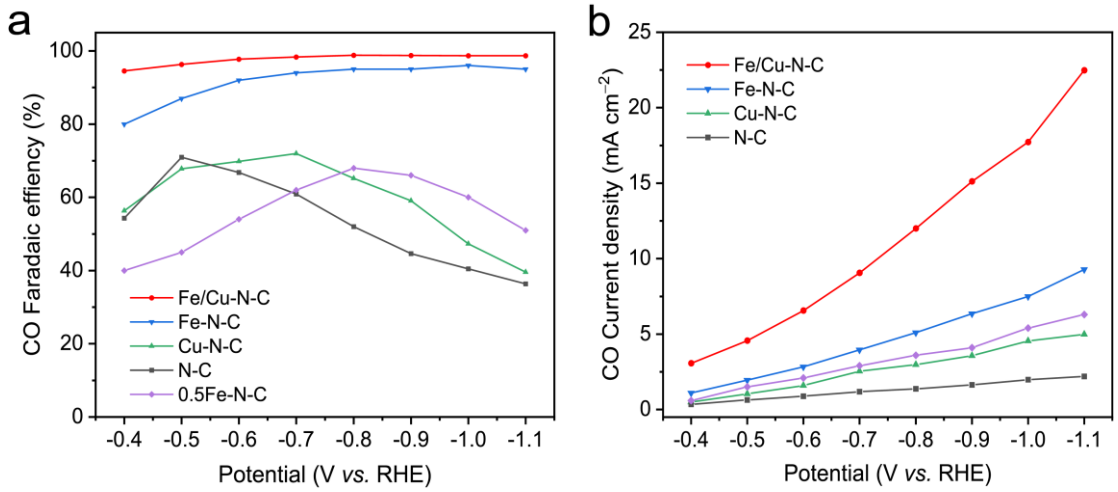

Fig. S20. (a) FE_{CO} and (b) j_{CO} of Fe/Cu-N-C, Fe-N-C, Cu-N-C, N-C and 0.5Fe-N-C at potentials from -0.4 to -1.1 V.

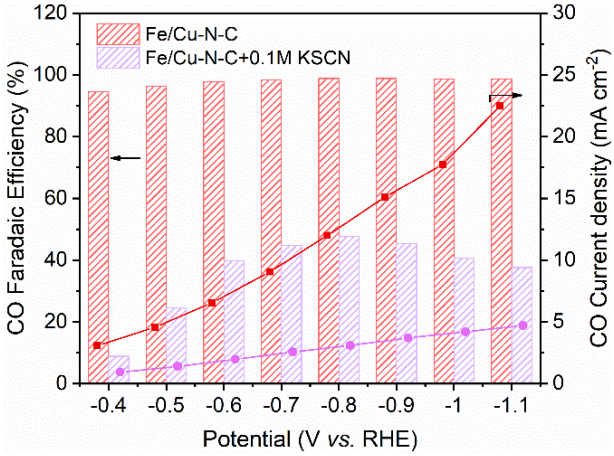

Figure S21. CO Faradaic efficiency and CO current density of Fe/Cu-N-C with and without 0.1 M KSCN solution.

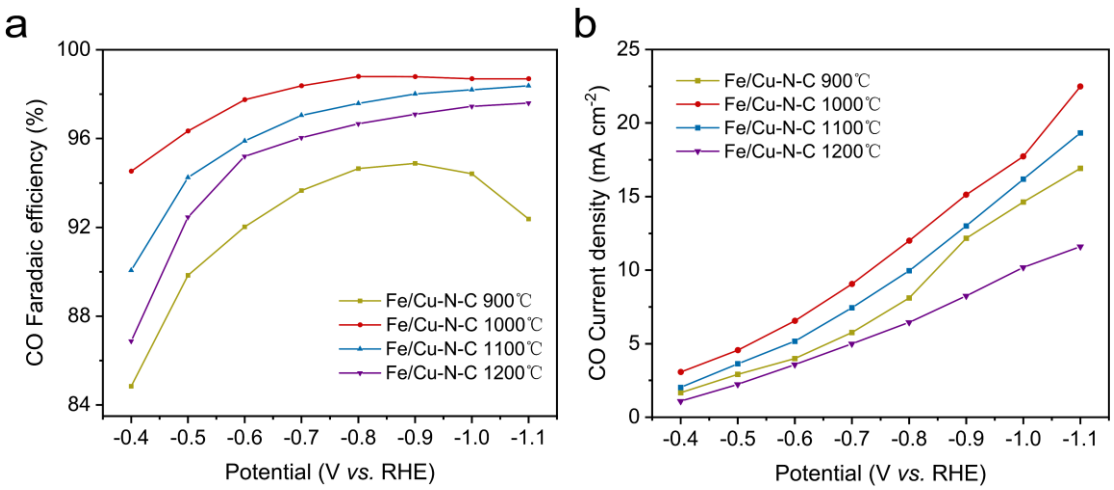

Fig. S22. Catalytic performance. (a) FE_{CO} and (b) CO current density of Fe/Cu-N-C (*T*) at various applied potentials.

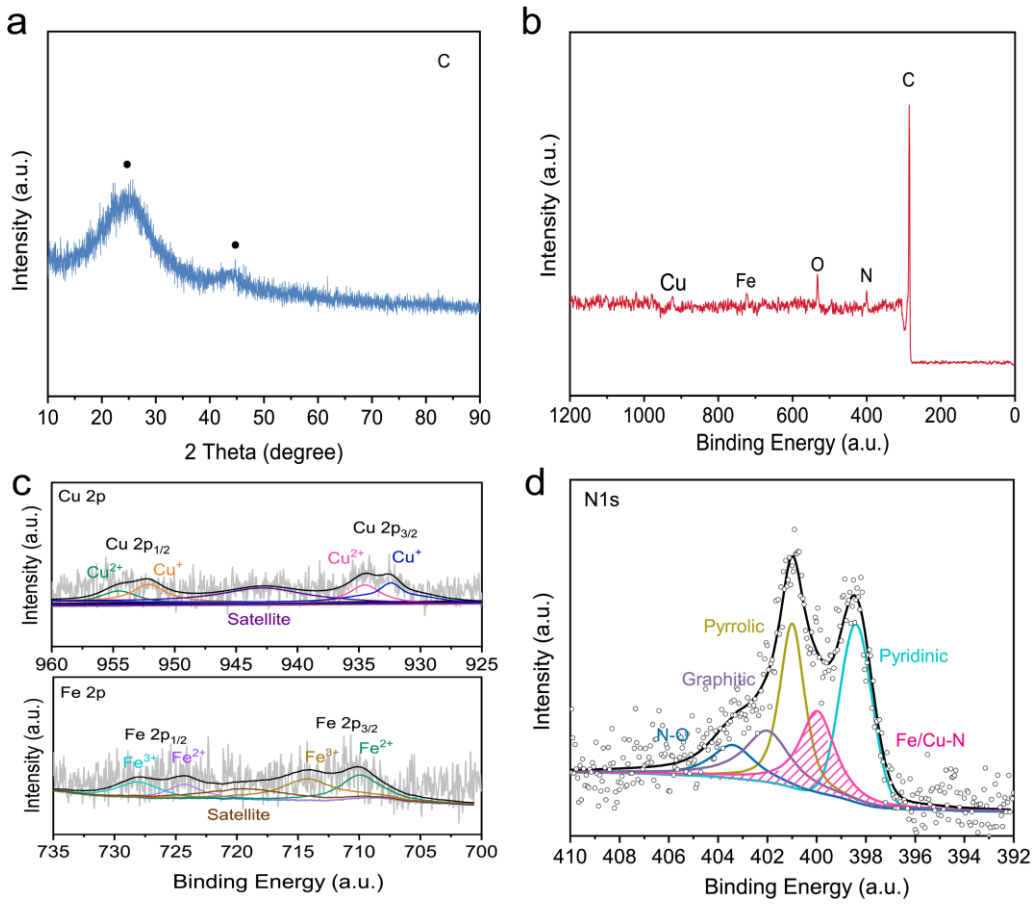

Fig. S23. (a) XRD pattern, (b) XPS survey spectrum, (c) high-resolution Cu 2p and Fe 2p XPS spectrum, and (d) high-resolution N 1s XPS spectrum of Fe/Cu-N-C after stability test for 60-hour.

Table S9. Elemental quantification of Fe/Cu-N-C measured by XPS.

Sample	C (at%)	N (at%)	O (at%)	Cu (at%)	Fe (at%)
Fe/Cu-N-C (before stability test)	89.14	5.70	4.69	0.18	0.29
Fe/Cu-N-C (after stability test)	89.61	5.03	4.97	0.15	0.24

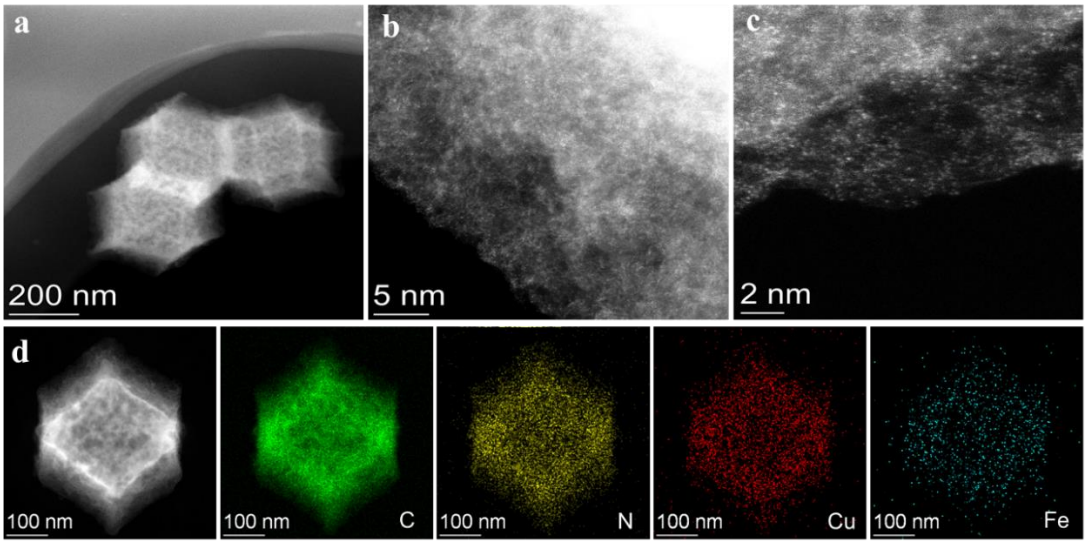

Fig. S24. (a), (b), (c) HAADF-STEM image of Fe/Cu-N-C, and (d) the corresponding EDS images after stability test for 60-hour.

Table S10. Catalytic performance of previously reported CO_2RR electrocatalysts and Fe/Cu-N-C.

Catalyst	Loading		E (V *vs.* RHE)	FE_{CO} (%)	*j* (mA cm^{-2})	Electrolyte	Reference
	mg cm^{-2}	wt%					
Cu-N_2/GN	0.5	1.45	−0.50	81	1.81	0.1 M $NaHCO_3$	[1]
Fe/NC-750	1	1.25	−0.60	80	1.9	0.1 M $KHCO_3$	[2]
Ni-N-C	0.5	0.4	−0.67	93	3.9	0.5 M $KHCO_3$	[3]
Fe-N-C	0.6	-	−0.58	93	2.8	0.1 M $KHCO_3$	[4]
Co-N_4	2	0.63	−0.80	82	10.9	0.1 M $KHCO_3$	[5]
ZnNx/C	1	0.1	−0.43	95	4.8	0.5 M $KHCO_3$	[6]
Cu-APC	1.5	1	−0.78	92	8.6	0.2 M $NaHCO_3$	[7]
NiN-GS	0.4	-	−0.82	93	4.0	0.1 M $KHCO_3$	[8]
Ni SAs/N-C	0.2	1.53	−1.0	72	10.5	0.5 M $KHCO_3$	[9]
AuCu NP	0.4	N/A	−0.77	80	1.39	0.1 M $KHCO_3$	[10]
Cu/$Ni(OH)_2$	0.5	0.92	−0.50	92	3.96	0.5 M $NaHCO_3$	[11]
CuFe-N-C	0.1	2.26	−0.50	95.5	2.10	0.5 M $KHCO_3$	[12]
Ni/Fe-N-C	0.5	1.31	−0.70	98	7.40	0.5 M $KHCO_3$	[13]
Fe/Cu-N-C	1	0.49	−0.40	95	3.26	0.1 M $KHCO_3$	This work
Fe/Cu-N-C	1	0.49	−0.60	98	6.74	0.1 M $KHCO_3$	This work
Fe/Cu-N-C	1	0.49	−0.80	99	12.91	0.1 M $KHCO_3$	This work

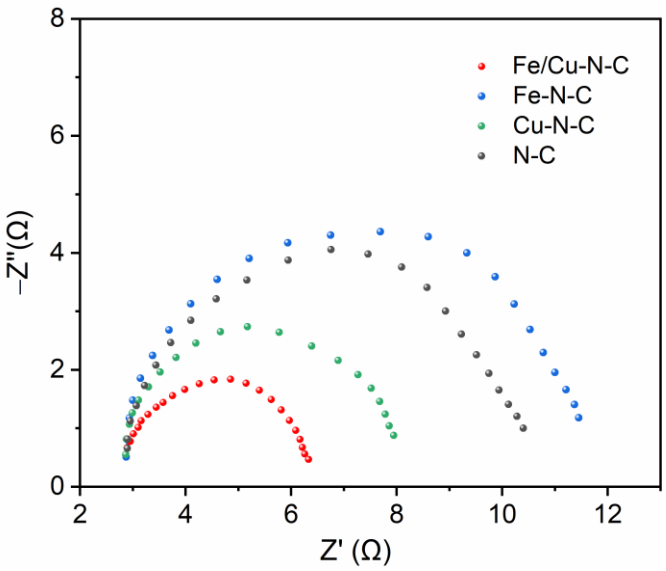

Fig. S25. Nyquist plots of the catalyst samples in the frequency range of 0.1 to 100000 Hz.

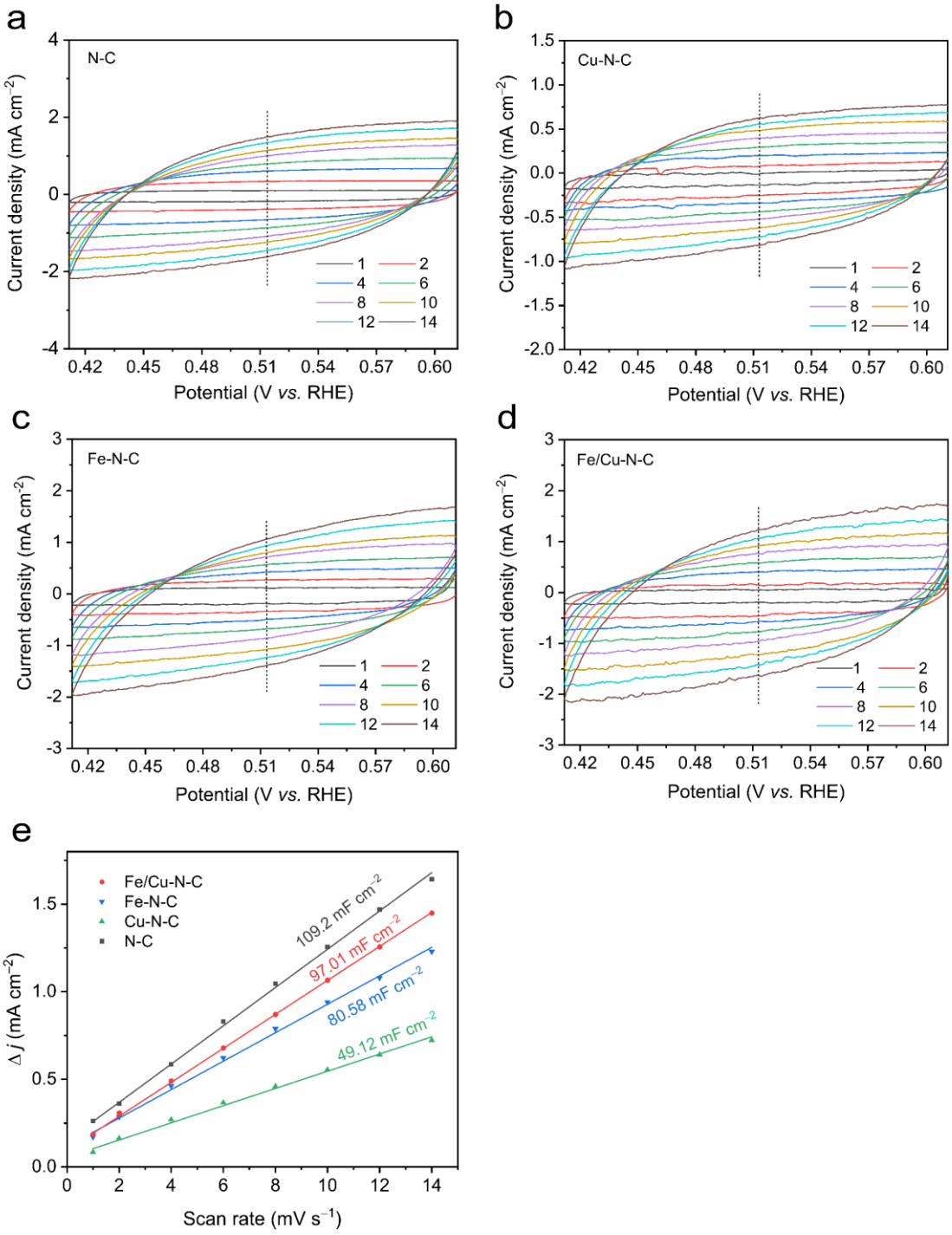

Fig. S26. Cyclic voltammograms measured at various scan rates (1, 2, 4, 6, 8, 10, 12, and 14 mV s^{-1}) for (a) N-C, (b) Cu-N-C, (c) Fe-N-C, and (d) Fe/Cu-N-C; (e) electrochemically active surface areas (ECSAs) estimated from the double-layer capacitances (C_{dl}) of the samples.

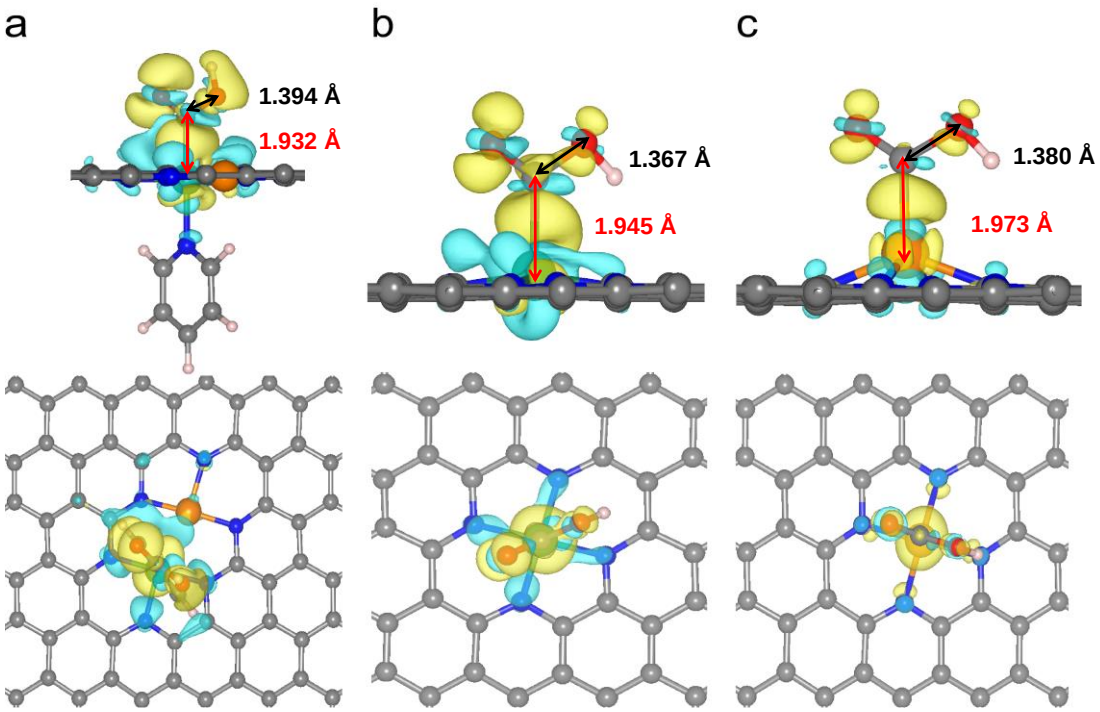

Fig. S27. Top and side view of net spin densities for (a) $N_4Fe\text{-}CuN_3$, (b) $Fe\text{-}N_4$, and (c) $Cu\text{-}N_4$ at an isosurface value of 1×10^{-3} eÅ^{-3}. The yellow and blue areas represent charge accumulation and depletion, respectively.

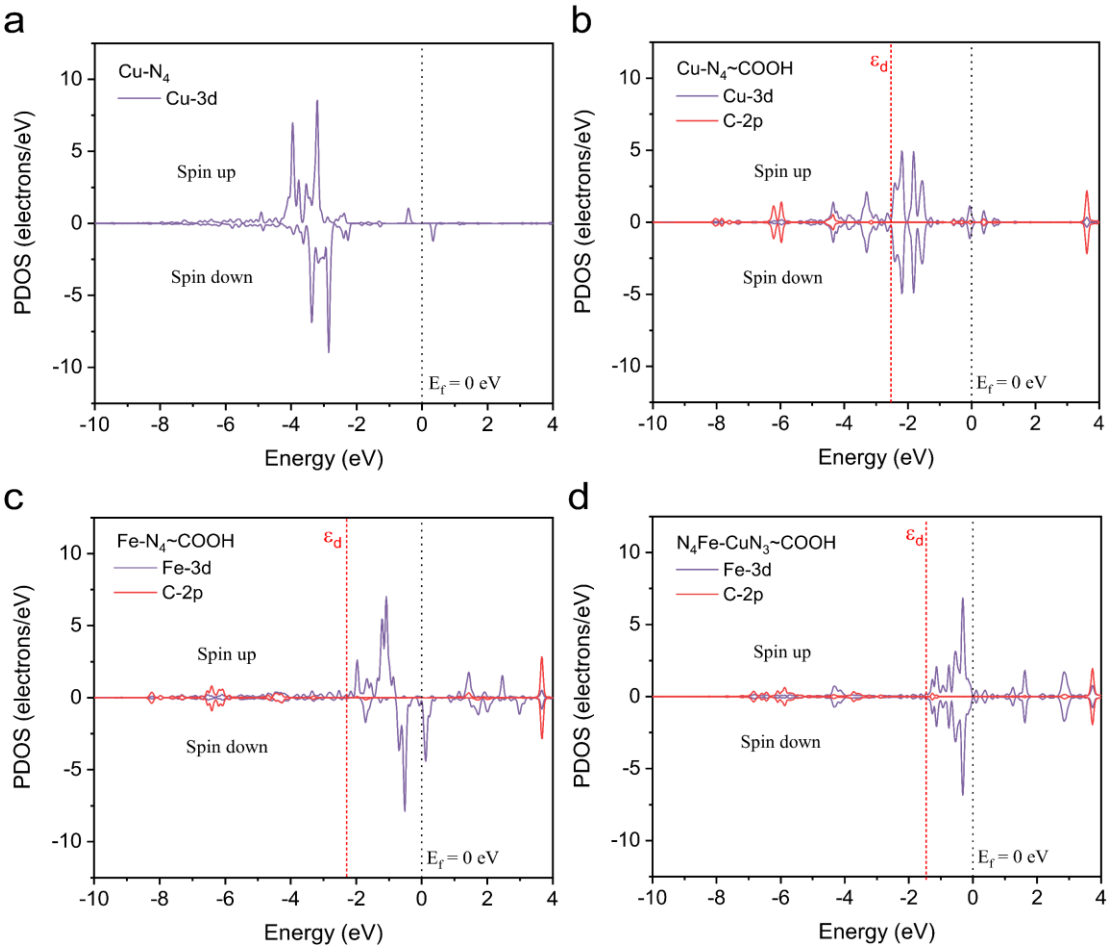

Fig. S28. Calculated partial density of states (PDOS) for (a) Cu-N_4 and for (b) Cu-N_4, (c) Fe-N_4, and (d) N_4Fe-CuN_3 with *COOH adsorption.

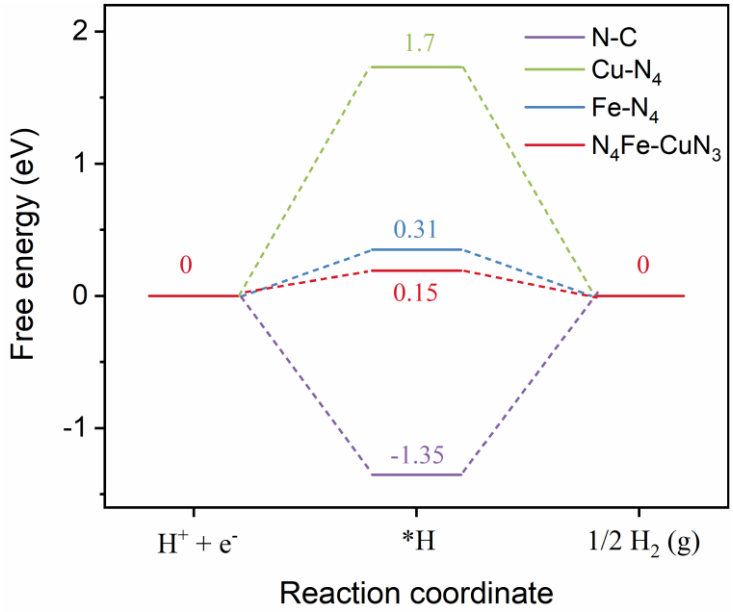

Fig. S29. Free energy diagram for the hydrogen evolution reaction on Cu-N_4, Fe-N_4, N-C, and N_4Fe-CuN_3 moieties at U = 0 V *vs.* RHE.

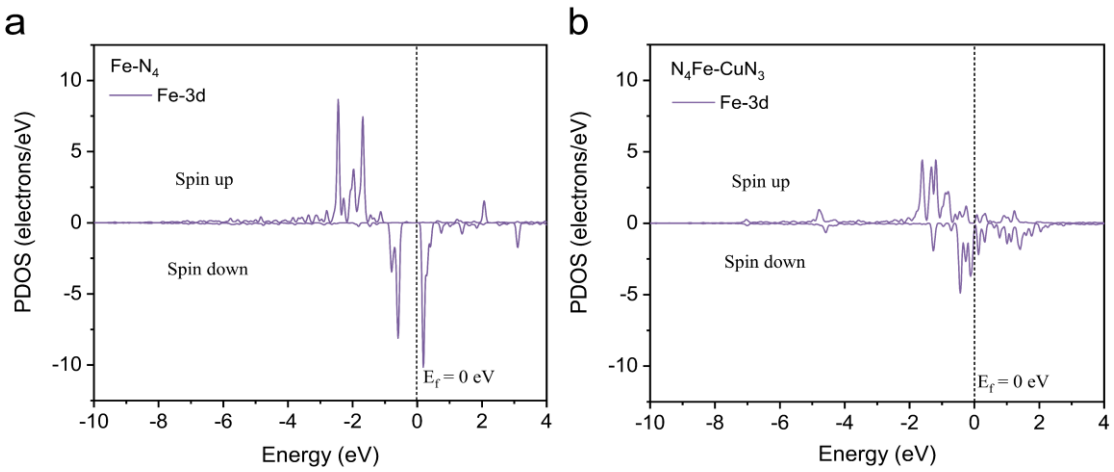

Fig. S30. Calculated partial density of states (PDOS) for (a) Fe-N_4 and (b) N_4Fe-CuN_3.

References

1. W. Zheng, J. Yang, H. Chen, Y. Hou, Q. Wang, M. Gu, F. He, Y. Xia, Z. Xia, Z. Li, B. Yang, L. Lei, C. Yuan, Q. He, M. Qiu and X. Feng, *Advanced Functional Materials*, 2019, **30**, 1907658.

2. C. H. Zhang, S. Z. Yang, J. J. Wu, M. J. Liu, S. Yazdi, M. Q. Ren, J. W. Sha, J. Zhong, K. Q. Nie, A. S. Jalilov, Z. Y. Li, H. M. Li, B. I. Yakobson, Q. Wu, E. L. Ringe, H. Xu, P. M. Ajayan and J. M. Tour, *Adv Energy Mater*, 2018, **8**, 1703487.

3. X. M. Hu, H. H. Hval, E. T. Bjerglund, K. J. Dalgaard, M. R. Madsen, M. M. Pohl, E. Welter, P. Lamagni, K. B. Buhl, M. Bremholm, M. Beller, S. U. Pedersen, T. Skrydstrup and K. Daasbjerg, *Acs Catalysis*, 2018, **8**, 6255-6264.

4. F. P. Pan, H. G. Zhang, K. X. Liu, D. Cullen, K. More, M. Y. Wang, Z. X. Feng, G. F. Wang, G. Wu and Y. Li, *Acs Catalysis*, 2018, **8**, 3116-3122.

5. Z. G. Geng, Y. J. Cao, W. X. Chen, X. D. Kong, Y. Liu, T. Yao and Y. Lin, *Applied Catalysis B-Environmental*, 2019, **240**, 234-240.

6. F. Yang, P. Song, X. Liu, B. Mei, W. Xing, Z. Jiang, L. Gu and W. Xu, *Angew Chem Int Ed Engl*, 2018, **57**, 12303-12307.

7. J. Jiao, R. Lin, S. Liu, W. C. Cheong, C. Zhang, Z. Chen, Y. Pan, J. Tang, K. Wu, S. F. Hung, H. M. Chen, L. Zheng, Q. Lu, X. Yang, B. Xu, H. Xiao, J. Li, D. Wang, Q. Peng, C. Chen and Y. Li, *Nat Chem*, 2019, **11**, 222-228.

8. K. Jiang, S. Siahrostami, A. J. Akey, Y. B. Li, Z. Y. Lu, J. Lattimer, Y. F. Hu, C. Stokes, M. Gangishetty, G. X. Chen, Y. W. Zhou, W. Hill, W. B. Cai, D. Bell, K. R. Chan, J. K. Norskov, Y. Cui and H. T. Wang, *Chem*, 2017, **3**, 950-960.

9. C. Zhao, X. Dai, T. Yao, W. Chen, X. Wang, J. Wang, J. Yang, S. Wei, Y. Wu and Y. Li, *J Am Chem Soc*, 2017, **139**, 8078-8081.

10. D. Kim, C. Xie, N. Becknell, Y. Yu, M. Karamad, K. Chan, E. J. Crumlin, J. K. Norskov and P. Yang, *J Am Chem Soc*, 2017, **139**, 8329-8336.

11. L. Dai, Q. Qin, P. Wang, X. Zhao, C. Hu, P. Liu, R. Qin, M. Chen, D. Ou, C. Xu, S. Mo, B. Wu, G. Fu, P. Zhang and N. Zheng, *Sci Adv*, 2017, **3**, e1701069.

12. F. Wang, H. Xie, T. Liu, Y. Wu and B. Chen, *Applied Energy*, 2020, **269**, 115029.

13. W. Ren, X. Tan, W. Yang, C. Jia, S. Xu, K. Wang, S. C. Smith and C. Zhao, *Angew Chem Int*

Ed Engl, 2019, **58**, 6972-6976.